The Astrophysical Journal, 672:1043–1053, 2008 January 10
© 2008. The American Astronomical Society. All rights reserved. Printed in U.S.A.

# $\nu$-PROCESS NUCLEOSYNTHESIS IN POPULATION III CORE-COLLAPSE SUPERNOVAE

Takashi Yoshida,[1] Hideyuki Umeda,[2] and Ken'ichi Nomoto[2,3]
*Received 2007 March 7; accepted 2007 September 20*


## ABSTRACT

We investigate the effects of neutrino-nucleus interactions (the $\nu$-process) on the production of iron-peak elements in Population III core-collapse supernovae. The $\nu$-process and the following proton and neutron capture reactions produce odd-$Z$ iron-peak elements in the complete and incomplete Si-burning region. This reaction sequence enhances the abundances of Sc, Mn, and Co in the supernova ejecta. Supernova explosion models of 15 and 25 $M_\odot$ stars with the $\nu$-process reproduce well the average Mn/Fe ratio observed in extremely metal-poor halo stars. In order to reproduce the observed Mn/Fe ratio, the total neutrino energy in the supernovae should be $(3-9)\times10^{53}$ ergs. Stronger neutrino irradiation and other production sites are necessary to reproduce the observed Sc/Fe and Co/Fe ratios, although these ratios increase by the $\nu$-process.


*Subject headings:* Galaxy: halo — neutrinos — nuclear reactions, nucleosynthesis, abundances — supernovae: general

## 1. INTRODUCTION

The abundance-metallicity relation of low-mass, extremely metal-poor (EMP) stars ($-4 \lesssim [\mathrm{Fe/H}] \lesssim -3$; $[\mathrm{X/Y}] \equiv \log(N_\mathrm{X}/N_\mathrm{Y}) - \log(N_\mathrm{X}/N_\mathrm{Y})_\odot$ where $N_\mathrm{X}$ and $N_\mathrm{Y}$ are the abundances of elements X and Y, respectively) and very metal-poor (VMP) stars ($-3 \lesssim [\mathrm{Fe/H}] \lesssim -2$) has been clarified by observations of very high quality spectra (e.g., Norris et al. 2001; Cayrel et al. 2004). This relation is expected to provide information on the supernovae (SNe) of Population III (first generation) massive stars (e.g., Nomoto et al. 2006) and the first stage of Galactic chemical evolution (GCE; e.g., Kobayashi et al. 2006). EMP stars are considered to have suffered the injection of heavy elements from one or a few SNe (e.g., Shigeyama & Tsujimoto 1998). The interstellar medium in a halo gradually becomes homogeneous in metallicity (Argast et al. 2000). Although studies of star formation in the first stage of GCE are in progress, the characteristics of first-generation stars, such as the initial mass function, have not been clarified. In order to clarify such characteristics, we should investigate nucleosynthesis in the candidates of first-generation stars, as well as the observed variations of the abundance distributions of EMP and VMP stars.

Recent observations have indicated that the abundance ratios [X/Fe] averaged over metal-poor stars with $-4 \lesssim [\mathrm{Fe/H}] \lesssim -2$ are between $-0.5$ and 0.5 for most observed elements (Cayrel et al. 2004). Their scatter around the average values deduced from new observations is much smaller than found in earlier studies. The elemental abundance distribution of metal-poor stars is not so different from that of the solar-system composition. Therefore, the small scatter is considered to suggest a primordial burst of high-mass stars or the very rapid mixing of matter from different bursts of early star formation.

From a theoretical viewpoint, Tominaga et al. (2007b) compared Population III hypernova (HN) yields with the abundance pattern of EMP stars with the metallicity range $-4.2 < [\mathrm{Fe/H}] < -3.5$ in Cayrel et al. (2004). They adopted the mixing-fallback model for the HNe. The HN yields give good agreement with the observed abundances for C, Na, Mg, Al, Si, Ca, Ni, and Zn. They also compared Population III SN and HN yields integrated over the Salpeter initial mass function (IMF) with the abundances of VMP stars in the metallicity range $-2.7 < [\mathrm{Fe/H}] < -2.0$ in Cayrel et al. (2004). They reproduced the observed trends of abundance ratios for C, O, Na, Mg, Al, Si, Ca, Cr, Ni, and Zn. The SN and HN yields of N, K, Sc, Ti, Mn, and Co are too small to explain the observed yield ratios, although Sc and Ti may be improved in high-entropy explosion models. The yields of Mn and Co may be reproduced by modification of the electron fraction $Y_e$, the value of which is still uncertain in the innermost region of SNe and HNe. Additional nucleosynthesis processes also remain open for these elements.

During a SN explosion, the collapsed core attains an extremely high temperature and high density, and neutrinos are produced through pair creation. The neutrinos are almost thermalized by neutrino-nucleus scattering at the center. They leave through the neutrinosphere, carrying away the gravitational binding energy of the core. The neutrino irradiation lasts for about $\sim$10 s. The total number of neutrinos emitted in a SN is very huge, i.e., about $N_\nu \sim 10^{58}$. The neutrinos interact with nuclei in the surrounding stellar material to produce new species of nuclei. This is called the $\nu$-process.

The $\nu$-process is expected to be an important production process for some elements in Population III SN explosions. The $\nu$-process is important for the synthesis of light elements, Li and B (Domogatsky et al. 1978; Woosley et al. 1990; Woosley & Weaver 1995, hereafter WW95; Yoshida et al. 2004, 2005a, 2006a, 2006b) and F (e.g., Woosley et al. 1990; WW95), and some heavy neutron-deficient nuclei such as $^{138}$La and $^{180}$Ta (Goriely et al. 2001; Heger et al. 2005). The $\nu$-process products are synthesized through spallations by neutrinos from abundant seed nuclei. The $\nu$-process also produces protons and neutrons, and their capture reactions also enhance the abundances of some elements. For Population III SNe, the seed nuclei are $\alpha$-nuclei abundantly produced in complete and incomplete Si burning during the explosions. Thus, the $\nu$-process in Population III SNe produces some additional odd-$Z$ elements.

We note that most of the nucleosynthesis calculations including the $\nu$-process have been carried out using spherical explosion models (WW95; Yoshida et al. 2005b). Although the total neutrino

[1] National Astronomical Observatory of Japan, Mitaka, Tokyo 181-8588, Japan; takashi.yoshida@nao.ac.jp.
[2] Department of Astronomy, School of Science, University of Tokyo, Tokyo 113-0033, Japan.
[3] Institute for the Physics and Mathematics of the Universe, University of Tokyo, Chiba 277-8582, Japan.

energy should be close to the gravitational binding energy released from the collapsing core, the properties of the neutrinos are still uncertain. The properties strongly depend on the explosion mechanism, but details of the mechanism have not been clarified. On the other hand, aspherical explosions have been investigated recently (e.g., Kotake et al. 2004; Scheck et al. 2004). In such a case, an aspherical structure for the neutrinosphere can be formed, but the properties of the neutrinos are still uncertain. Therefore, the dependence of the abundances of Population III SNe and HNe on neutrino properties should be investigated.

In this study we focus on the effect of the $\nu$-process on the production of odd-$Z$ iron-peak elements, Sc, Mn, and Co, during Population III SN and HN explosions. We calculate the SN nucleosynthesis including the $\nu$-process. Then we investigate the dependence of the abundances of Sc, Mn, and Co in the SN ejecta on the energy of the neutrinos, the stellar mass, and the explosion energy. Sc, Mn, and Co are expected to be at least partly synthesized through the $\nu$-process. We also indicate whether the abundance ratios of Sc, Mn, and Co to Fe reproduce those observed in EMP stars when we take into account the $\nu$-process.

In § 2 we explain the stellar evolution models and explosion models for two SNe and one HN. We also describe the nucleosynthesis models including the $\nu$-process and the neutrino irradiation models. In § 3 we show the abundance distributions of Sc, Mn, and Co in the ejecta of the SN and HN models. We explain additional production of these elements through the $\nu$-process. In § 4 we explain the effect of the $\nu$-process on the abundance ratios of Sc, Mn, and Co to Fe and the dependence on the neutrino irradiation strength. We also compare our results with the abundance ratios observed in EMP stars. In § 5 we discuss other production processes of Sc, Mn, and Co proposed in recent studies and the effect of the $\nu$-process. Finally, we summarize this study in § 6.

## 2. SN EXPLOSION MODELS FOR POPULATION III MASSIVE STARS

### 2.1. *Stellar Evolution and SN Explosion Models*

We calculate the evolution of Population III stars for initial masses of 15 and 25 $M_\odot$ from zero-age main sequence to the onset of core collapse. We use a Henyey-type stellar evolution code including a nuclear reaction network with about 300 isotopes to calculate detailed nucleosynthesis and energy generation. The input physics is the same as for the models used in Umeda & Nomoto (2002). SN explosions are calculated using a hydrodynamical code based on a spherically symmetrical piecewise parabolic method (Colella & Woodward 1984).

We set the explosion energy of the 15 and 25 $M_\odot$ SN models to be $E_{51} = 1$, where $E_{51}$ is the explosion energy in units of $1 \times 10^{51}$ ergs. We also calculate the explosion of a HN for a 25 $M_\odot$ star model with $E_{51} = 20$.

The location of the mass cut of the SN explosions is determined as follows. For the 15 $M_\odot$ star model, we set the location of the mass cut at $M_r = 1.71\ M_\odot$ ($M_r$ being the mass coordinate of the star) to obtain an ejected $^{56}$Ni mass of 0.07 $M_\odot$. In the case of the 25 $M_\odot$ SN, we set the mass cut location at $M_r = 1.92\ M_\odot$, so that large Co/Fe and Zn/Fe ratios are obtained. This location corresponds to the bottom of the layer where the electron fraction $Y_e$ is close to 0.5 (Umeda & Nomoto 2005; Tominaga et al. 2007b). A large amount of $^{56}$Ni is produced in the region of $1.92\ M_\odot \le M_r \le 2.2\ M_\odot$ (see § 3.2 for details). Since the location of the mass cut is deep, this model ejects a $^{56}$Ni mass of 0.36 $M_\odot$. This model corresponds to a SN with an explosion energy of $E_{51} \sim 1$, yielding a large amount of $^{56}$Ni [$M(^{56}\mathrm{Ni}) \sim 0.3\ M_\odot$], like SN 2005bf (Tominaga et al. 2005). Note that the mixing-fallback model is not applied to these cases.

TABLE 1
THE $^{56}$Ni MASS AND RATIOS [Sr/Fe], [Mn/Fe], AND [Co/Fe] OF POPULATION III SN AND HN MODELS

| $E_\nu$ (ergs) | $M(^{56}\mathrm{Ni})$ ($M_\odot$) | [Sc/Fe] | [Mn/Fe] | [Co/Fe] |
|---|---|---|---|---|
| | 15 $M_\odot$ SN | | | |
| No neutrinos | 0.072 | −1.46 | −0.53 | −1.10 |
| $3 \times 10^{53}$ | 0.072 | −1.21 | −0.29 | −0.73 |
| $9 \times 10^{53}$ | 0.071 | −0.99 | −0.04 | −0.34 |
| $3 \times 10^{54}$ | 0.068 | −0.69 | 0.36 | 0.16 |
| $3 \times 10^{53}$ ($T_\nu = 8$ MeV) | 0.072 | −1.15 | −0.20 | −0.58 |
| | 25 $M_\odot$ SN | | | |
| No neutrinos | 0.356 | −1.73 | −0.83 | −0.95 |
| $3 \times 10^{53}$ | 0.353 | −1.09 | −0.45 | −0.42 |
| $9 \times 10^{53}$ | 0.348 | −0.71 | −0.12 | −0.14 |
| $3 \times 10^{54}$ | 0.327 | −0.29 | 0.28 | 0.43 |
| $3 \times 10^{53}$ ($T_\nu = 8$ MeV) | 0.353 | −0.91 | −0.34 | −0.28 |
| | 25 $M_\odot$ HN | | | |
| No neutrinos | 0.065 | −1.13 | −1.85 | −0.13 |
| $3 \times 10^{53}$ | 0.065 | −1.00 | −1.45 | −0.19 |
| $9 \times 10^{53}$ | 0.065 | −0.81 | −1.12 | −0.23 |
| $3 \times 10^{54}$ | 0.064 | −0.44 | −0.61 | −0.25 |
| $3 \times 10^{53}$ ($T_\nu = 8$ MeV) | 0.065 | −0.92 | −1.32 | −0.14 |

In the case of the 25 $M_\odot$ HN model, we apply the mixing-fallback model (Umeda & Nomoto 2005; Tominaga et al. 2007b). This model approximates the aspherical effects of HN explosions (Tominaga et al. 2007a). During an aspherical explosion, the central core of the star collapses first. Then, a jetlike explosion ejects the surrounding stellar materials. Some of the materials in the inner region may fall back to the central core from an off-axis direction of the jet. There are three parameters in the mixing-fallback model; the initial mass cut $M_{\mathrm{cut}}$(ini), the outer boundary of the mixing region $M_{\mathrm{mix}}$(out), and the ejection factor $f$. The initial mass cut corresponds to the mass of the initially collapsing core. The outer boundary of the mixing region corresponds to the location where the surrounding materials infall to the core during the explosion. The ejection fraction is the fraction of ejected material in the mixing region. Details of the mixing-fallback model have been described in Tominaga et al. (2007b).

The values of the mixing-fallback parameters should be related to the explosion features such as asphericity and energy deposition rate (Tominaga et al. 2007a). However, the explosion mechanism has not been clarified. Therefore, we determine these parameter values in a way similar to case A in Tominaga et al. (2007b). The location of the initial mass cut is set as $M_{\mathrm{cut}}(\mathrm{ini}) = 1.92\ M_\odot$, which is the bottom of the $Y_e \sim 0.5$ layer. This condition produces a large Zn/Fe ratio (Umeda & Nomoto 2002, 2005). The outer boundary of the mixing region is determined to be $M_{\mathrm{mix}}(\mathrm{out}) = 3.83\ M_\odot$, where the mass fraction of $^{56}$Ni decreases to $10^{-3}$. The ejection factor is determined to be $f = 0.065$ in order to yield [O/Fe] = 0.5. The electron fraction in the complete and incomplete Si-burning regions is not modified in this study. The $^{56}$Ni mass of each explosion model is listed in Table 1.

### 2.2. *SN Neutrinos and Nucleosynthesis Models*

A huge amount of neutrinos are emitted during SN explosions. For spherically symmetrical SN explosions, neutrinos are emitted

isotropically from the neutrinosphere and carry away the majority of the gravitational energy of the proto–neutron star. On the other hand, aspherical SNe and a jetlike explosion would emit neutrinos anisotropically. In this case neutrino irradiation may be very strong in a specific direction. Since we assume spherically symmetrical SN explosions, we assume isotropic neutrino emission.

The strength of the neutrino flux is determined by the total neutrino energy. The adopted values of the total neutrino energy are $E_\nu = 3\times10^{53}$, $9\times10^{53}$, and $3\times10^{54}$ ergs. The first value corresponds to normal neutrino irradiation and is almost equal to the gravitational binding energy of a 1.4 $M_\odot$ neutron star (Lattimer & Prakash 2001). We assume that the neutrino luminosity decreases exponentially with time. The decay time of the neutrino luminosity is set to be 3.0 s.

The spectra of the SN neutrinos are assumed to obey Fermi distribution with zero chemical potentials. The temperatures of $\nu_{\mu,\tau}$, $\bar{\nu}_{\mu,\tau}$ and $\nu_e$, $\bar{\nu}_e$ are set to be $T_\nu = 6$ MeV/$k$ and 4 MeV/$k$, respectively. This set of neutrino temperatures is the same as in Rauscher et al. (2002) and Yoshida et al. (2005b). We note that WW95 provided SN yields adopting $\nu_{\mu,\tau}$ and $\bar{\nu}_{\mu,\tau}$ temperatures of $T_\nu = 8$ MeV and $E_\nu = 3\times10^{53}$ ergs. Therefore, we briefly mention the yields obtained using this parameter set. Detailed nucleosynthesis during the SN explosions is calculated by post-processing using a code of Hix & Thielemann (1996) to which the $\nu$-process reactions in Yoshida et al. (2005b) were added.

We should note that the evolution of the neutrino luminosity and energy spectra of HNe may be different from that of SNe. The neutrino emission from rapidly accreting disks surrounding black holes during gamma-ray bursts and HNe has been investigated (e.g., McLaughlin & Surman 2007). It was shown that $\nu_e$ and a smaller amount of $\bar{\nu}_e$ are mainly emitted from the accretion disks with slightly harder energy spectra than those from proto–neutron stars. However, the evolution of neutrino emission during HN explosions is still largely uncertain. On the other hand, the main contribution of the $\nu$-process is neutral-current interactions, which do not depend on neutrino flavors (WW95; Yoshida et al. 2004). Furthermore, the yields of the $\nu$-process products depend on both neutrino energy spectra and the total neutrino energy. Roughly speaking, a larger total neutrino energy corresponds to harder neutrino energy spectra (Yoshida et al. 2005a). Therefore, we set the total neutrino energy as a parameter.

The value of the total neutrino energy, $E_\nu = 3\times10^{54}$ ergs, may be too large even in the HN model. If an element is not produced abundantly through the $\nu$-process even at $E_\nu = 3\times10^{54}$ ergs, the $\nu$-process contribution in general should be very small for the production of the element.

## 3. ABUNDANCE DISTRIBUTIONS OF Sc, Mn, AND Co

### 3.1. 15 $M_\odot$ *Supernova*

We explain the mass fractions of Sc, Mn, and Co, as well as the contribution of the $\nu$-process for their production. Figure 1*a* shows the distributions of the mass fractions of Sc, Mn, and Co in the 15 $M_\odot$ SN model without taking into account the $\nu$-process. In this figure, the main product in the range of 1.71 $M_\odot \le M_r \le$ 1.74 $M_\odot$ is $^{56}$Ni. In this region a large amount of iron-peak elements are produced through complete Si burning. We call this region the Ni layer. In the region outside the Ni layer, incomplete Si burning occurs during the explosion, and a large amount of Si, as well as a smaller amount of iron-peak elements, is produced. We call this region (1.74 $M_\odot \le M_r \le$ 1.95 $M_\odot$) the Si/S layer.

The characteristics of the mass fractions and main production sites of Sc, Mn, and Co without the $\nu$-process are explained as follows.

1. A small mass fraction of Sc is produced at 1.86 $M_\odot \lesssim M_r \lesssim$ 1.95 $M_\odot$. The mass fraction is about $1\times10^{-6}$ at the maximum. Most of the Sc is produced through incomplete Si burning.
2. Most of the Mn is produced in the Si/S layer through incomplete Si burning. The mass fraction at the maximum is about $3\times10^{-3}$, which is much larger than that of Sc. Part of the Mn is also produced in the Ni layer, but the mass fraction is much smaller.
3. Co is also produced in the Ni layer. The mass fraction of Co is about $3\times10^{-4}$ throughout this layer.

Next we consider the effect of the $\nu$-process on the production of Sc, Mn, and Co. Figures 1*b* and 1*c* show the distributions of the mass fractions taking into account the $\nu$-process with $E_\nu = 3\times10^{53}$ and $3\times10^{54}$ ergs, respectively.

#### 3.1.1. Sc

We see that additional Sc is produced in the Si/S layer (1.9 $M_\odot \lesssim M_r \lesssim$ 1.95 $M_\odot$) and in the Ni layer. The mass fraction of Sc is less than $1\times10^{-6}$. Most of the Sc is first produced as $^{45}$Ti and $^{45}$V. In the Ni layer, a large amount of $^{44}$Ti is produced through complete Si burning. At the same time, $^{45}$Ti and $^{45}$V are partly produced through neutron and proton captures of $^{44}$Ti. Without the $\nu$-process, however, the produced $^{45}$Ti and $^{45}$V are smoothly captured or decomposed again during the explosion. Additional protons are produced through the $\nu$-process, so that some $^{45}$V is produced again by proton capture.

#### 3.1.2. Mn

We see an increase in the mass fraction of Mn in the Ni layer by about 3 orders of magnitude compared with the case without the $\nu$-process. The mass fraction in the Si/S layer also increases by about a factor of 1.4. During the SN explosion, Mn is produced as $^{55}$Co. The amount of $^{55}$Mn originally produced in the SN is much smaller. In the Si/S layer, $^{55}$Co is produced by $^{54}$Fe$(p,\gamma)^{55}$Co or photodisintegration from $^{56}$Ni. When the $\nu$-process is considered, $^{55}$Co is also produced through $^{56}$Ni$(\nu,\nu'p)^{55}$Co after the production of $^{56}$Ni through complete and incomplete Si burning. Since the decay time of the neutrino luminosity is longer than the timescale of Si burning, the neutrino irradiation proceeds after the cessation of Si burning.

#### 3.1.3. Co

When we consider the $\nu$-process, the mass fraction of Co increases by about a factor of 3 throughout the Ni layer. The main production region of Co does not change when we consider the $\nu$-process. Most of the Co is produced as $^{59}$Cu, and about 10% of the $^{59}$Co is produced as $^{59}$Ni. We see a similar increase in the mass fractions of $^{59}$Cu and $^{59}$Ni in the Ni layer. Most of the $^{59}$Cu and $^{59}$Ni are produced through the captures of protons and neutrons by $^{58}$Ni. The protons and neutrons are produced through the $\nu$-process even after the cessation of complete Si burning. Therefore, the additional production raises the mass fraction of Co.

#### 3.1.4. *Larger Neutrino Irradiation*

We also consider the case of larger neutrino irradiation with $3\times10^{53}$ ergs. The distributions of the mass fractions are shown in Figure 1*c*. We see that the mass fractions of Sc, Mn, and Co in the Ni layer are larger by a factor of 7–9 than those in the case of $E_\nu = 3\times10^{53}$ ergs. The dependence of the obtained mass fractions on the total neutrino energy is slightly less than linear. In this case all three elements are mainly produced in the Ni layer, although Mn is mainly produced in the Si/S layer in the former cases.

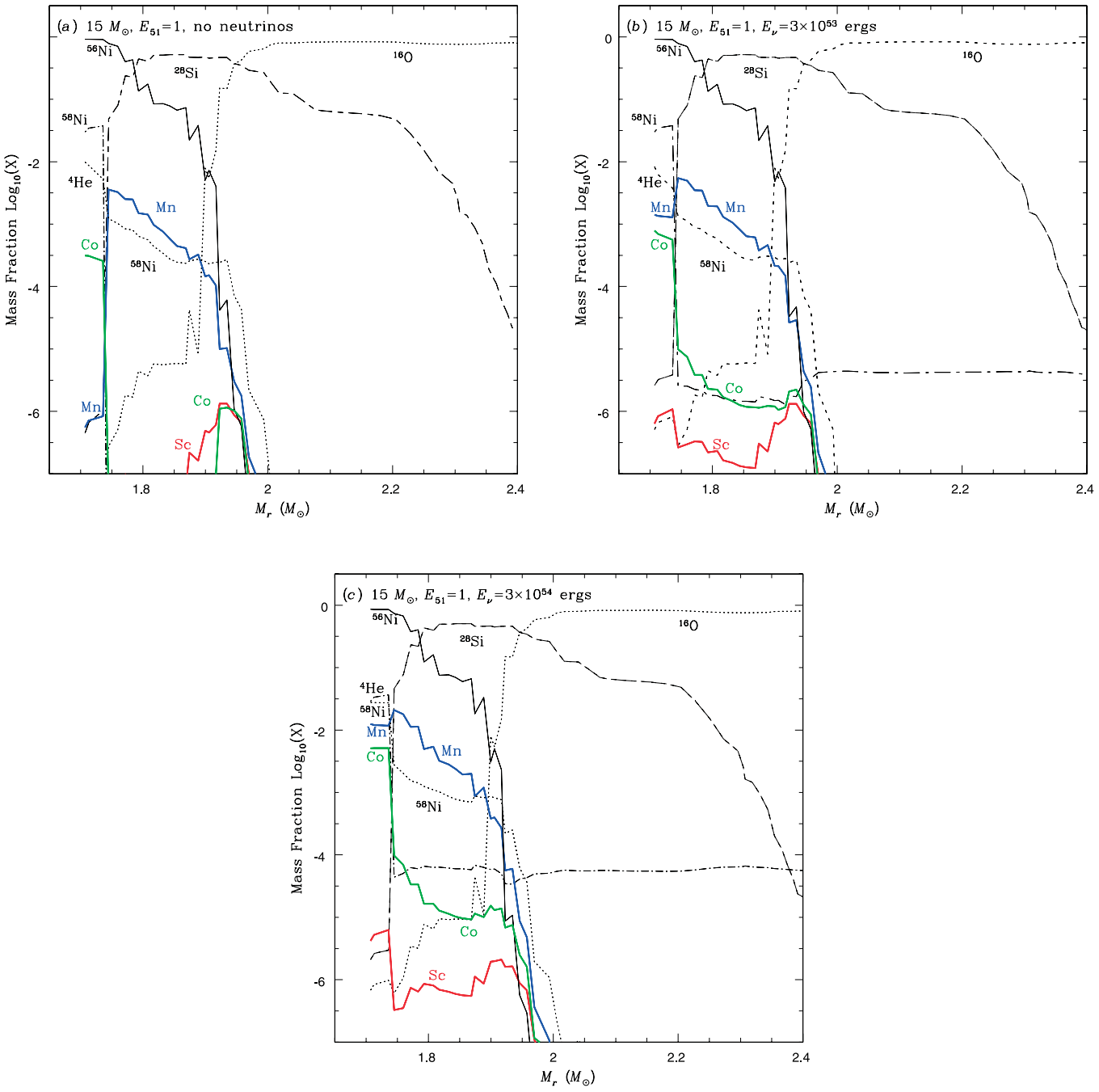


FIG. 1.—Mass fraction distribution after SN explosions of the 15 $M_\odot$ Population III star model in the cases of (*a*) the $\nu$-process unconsidered, (*b*) the $\nu$-process with $E_\nu = 3 \times 10^{53}$ ergs, and (*c*) the $\nu$-process with $E_\nu = 3 \times 10^{54}$ ergs. Red, blue, and green lines correspond to the mass fractions of Sc, Mn, and Co, respectively.

### 3.2. 25 $M_\odot$ *Supernova*

The mass fractions of the 25 $M_\odot$ SN model without the $\nu$-process are shown in Figure 2*a*. In this figure the Ni layer where complete Si burning occurs is in the range between 1.92 and 2.2 $M_\odot$ in the mass coordinate. The Si/S layer that suffers incomplete Si burning is between 2.2 and 2.75 $M_\odot$. The ejected masses of these layers are larger than the corresponding layers in the 15 $M_\odot$ SN model. The distributions of the mass fractions of Sc, Mn, and Co in the 25 $M_\odot$ SN model are roughly similar to those in the 15 $M_\odot$ SN model. Most of the Sc is produced in the outer part of the Si/S layer ($M_r = 2.6$–$2.75$ $M_\odot$). Mn is mainly produced in the Si/S layer too. Most of the Co is produced in the Ni layer.

The mass fractions of Sc, Mn, and Co with a $\nu$-process of $E_\nu = 3 \times 10^{53}$ ergs are shown in Figure 2*b*. When we consider the $\nu$-process, their increase is seen in the Ni layer. For Sc, the mass fraction reaches about $2 \times 10^{-6}$. It is about $1 \times 10^{-3}$ for Mn, but the main Mn production is still in the Si/S layer. An increase in abundance from the $\nu$-process is seen in the Si/S layer. For Co, the abundance increases by about a factor of 2.

The mass fractions of Sc, Mn, and Co in the case of a larger neutrino irradiation ($E_\nu = 3 \times 10^{54}$ ergs) are shown in Figure 2*c*. We obtain larger ones for Sc, Mn, and Co. The mass fraction of Sc in the Ni layer is about $2 \times 10^{-5}$, which is larger than that of the 15 $M_\odot$ SN. For Mn and Co, the abundances in the Ni layer are close to those of the 15 $M_\odot$ SN. The increase in the Mn abundance in the Si/S layer is also seen.

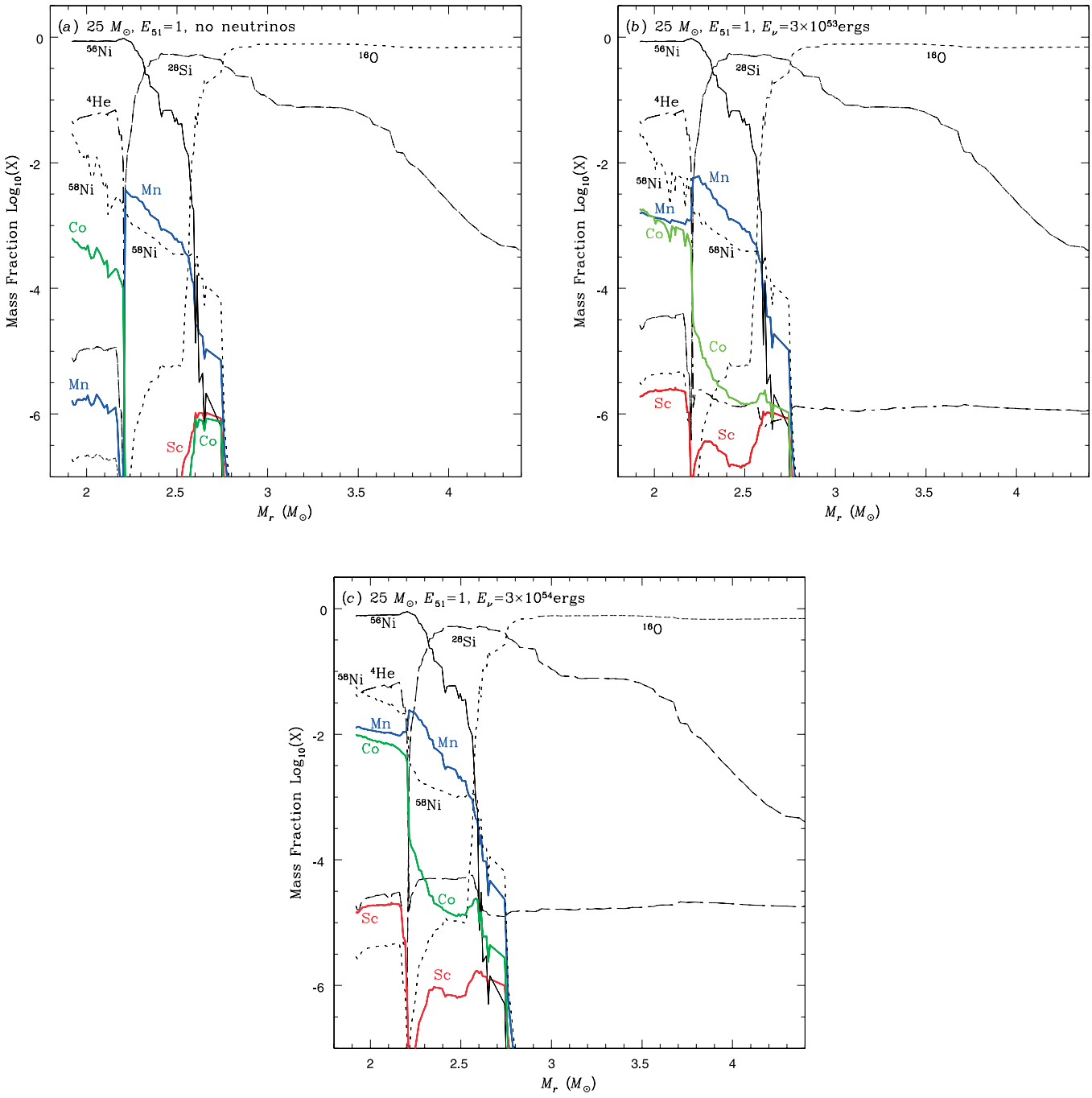


FIG. 2.—Same as Fig. 1, but for the SN explosion of the 25 $M_\odot$ Population III star model.

### 3.3. 25 $M_\odot$ *Hypernova*

We explain the effects of the $\nu$-process on the element production in the 25 $M_\odot$ HN model with $E_{51} = 20$. Figure 3*a* shows the distribution of the mass fractions in the 25 $M_\odot$ HN model without the $\nu$-process. The mass coordinate ranges of the Ni and Si/S layers are 1.92 $M_\odot \leq M_r \leq$ 3.0 $M_\odot$ and 3.0 $M_\odot \leq M_r \leq$ 3.8 $M_\odot$, respectively. The mass contained in each of the two layers for the 25 $M_\odot$ HN is larger than that of the corresponding layer of the 25 $M_\odot$ SN model. We see that the mass fractions of Sc, Mn, and Co in each burning region are not so different from those in the 25 $M_\odot$ SN; most of the Sc and Mn are produced in the Si/S layer, and Co is produced in the Ni layer. The average value of the Co mass fraction in the Ni layer is larger than that in the 25 $M_\odot$ SN.

The distributions of the mass fractions in the 25 $M_\odot$ HN model with the $\nu$-process ($E_\nu = 3 \times 10^{53}$ ergs) are shown in Figure 3*b*. An increase in the mass fraction from the $\nu$-process is mainly seen for Sc and Mn. As shown in the cases of the SNe, additional Sc is produced in the Ni layer. In addition, some Mn is also produced there. Since the range of the Ni layer is large, the contribution from the Ni layer is larger than that from the Si/S layer in this case. On the other hand, a clear effect of the $\nu$-process is not seen for Co.

Figure 3*c* shows the mass fractions in the 25 $M_\odot$ HN model with larger neutrino irradiation ($E_\nu = 3 \times 10^{54}$ ergs). As in the SN case, the Sc abundance in the Ni layer is larger by about a factor of 10 than that in the case of the normal neutrino irradiation ($E_\nu = 3 \times 10^{53}$ ergs). The mass fraction of Mn is similarly larger.

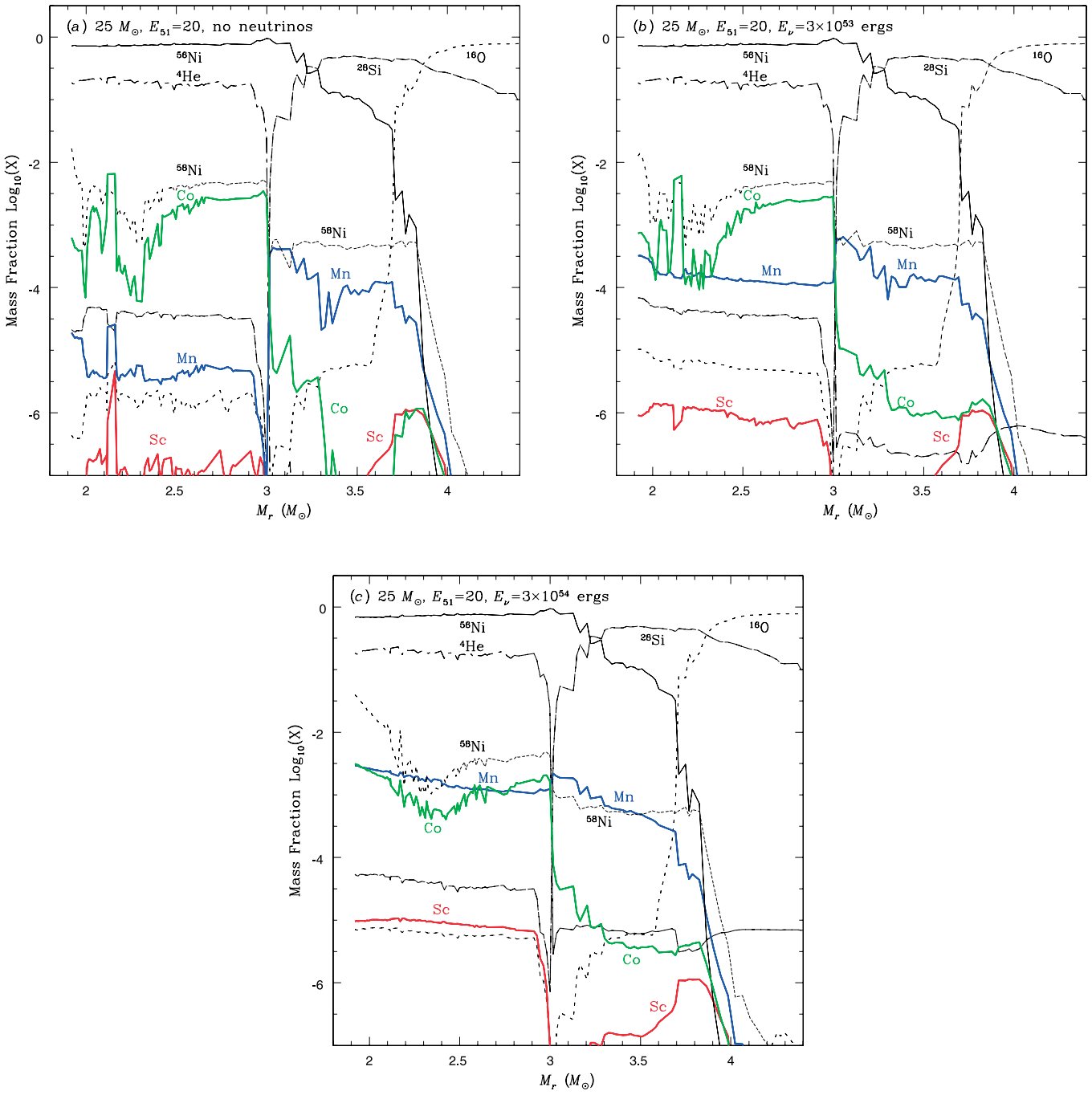


FIG. 3.—Same as Fig. 1, but for the HN explosion ($E_{51} = 20$) of the 25 $M_\odot$ Population III star model.

In the Si/S layer, the amount of Mn also increases. On the other hand, the mass fraction of Co does not change likewise, even with the large neutrino irradiation. Co is produced through complete Si burning in the Ni layer, and most of it is not decomposed during the explosion. Since HNe produce large amounts of Co even without neutrino irradiation (Umeda & Nomoto 2005), the additional production through the $\nu$-process hardly has an effect.

## 4. ABUNDANCE RATIOS OF Sc, Mn, AND Co

We have shown that some amounts of Sc, Mn, and Co are produced through the $\nu$-process and the following capture reactions of neutrons and protons. This additional production increases the total abundances of these elements in Population III SN and HN explosions. Next we show the distributions of the abundance ratios in the 15 and 25 $M_\odot$ SN and the 25 $M_\odot$ HN models. We also compare our results with the observed abundances of low-mass EMP stars. As a reference for the observed abundances, we use the abundance ratios to Fe averaged over the data of 22 low-mass halo stars with $[\mathrm{Fe/H}] \leq -3.0$ in Cayrel et al. (2004).

### 4.1. 15 $M_\odot$ *Supernova*

We show the abundance ratios in the 15 $M_\odot$ SN model in Figure 4. The ratios of [Sc/Fe], [Mn/Fe], and [Co/Fe] are listed in Table 1. The abundance ratios of the three elements are much smaller than the corresponding solar ratios. For other elements, the abundance ratios of odd-$Z$ elements are smaller than those of neighboring even-$Z$ elements. When we consider the $\nu$-process, the ratios [Sc/Fe], [Mn/Fe], and [Co/Fe] increase by 0.24–0.37 dex

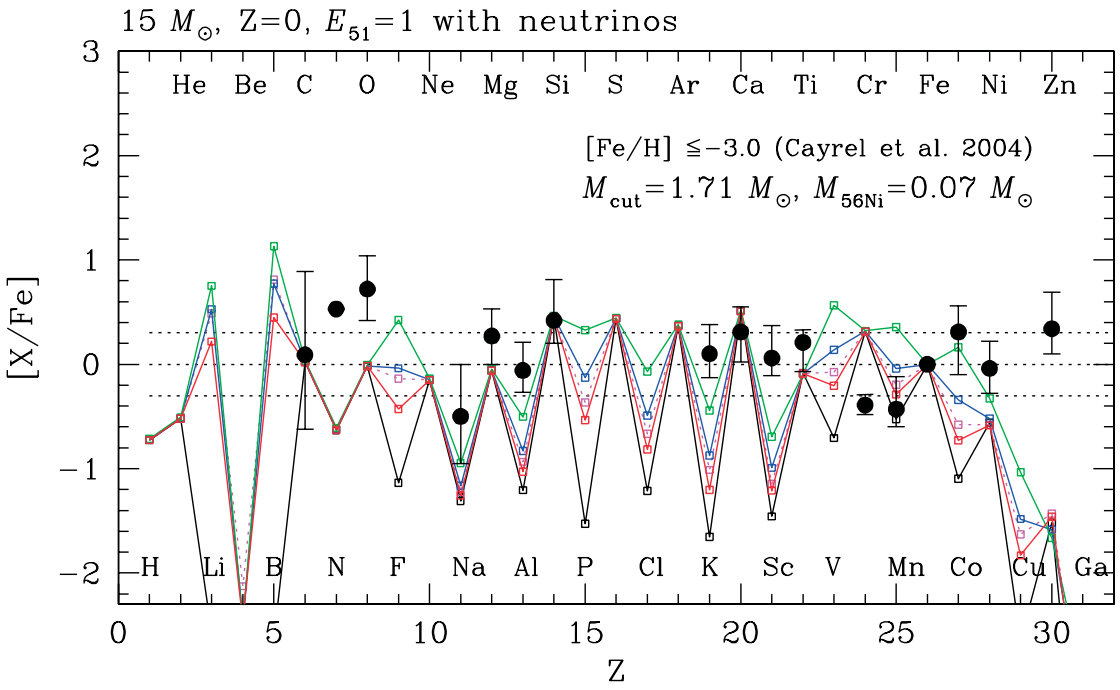


FIG. 4.—Abundance ratios to Fe in the SN of the 15 $M_\odot$ Population III star. The horizontal axis is the atomic number $Z$. The vertical axis is [X/Fe] (see text). The black, red, blue, and green lines indicate the abundance ratios in the cases without the $\nu$-process, and with the $\nu$-process and $E_\nu = 3\times10^{53}$, $9\times10^{53}$, and $3\times10^{54}$ ergs. The magenta dotted line indicates the case of the $\nu$-process and $(E_\nu, T_\nu) = (3\times10^{53}$ ergs, 8 MeV). The circles indicate the observed abundance ratios averaged over 22 halo stars with [Fe/H] $\leq -3.0$ in Cayrel et al. (2004). Error bars correspond to the abundance ratio ranges of these stars.

(see Table 1). Thus, the $\nu$-process raises the abundances of these elements. Since the Fe abundance is not altered by the $\nu$-process, the increase in the abundance ratios is due to the increase in the abundances by the $\nu$-process. A larger irradiation by neutrinos enhances the abundances of these elements. In the case of $3\times10^{54}$ ergs, the abundance ratios for Mn and Co are larger than the corresponding solar ratios (see Table 1 and Fig. 4). The abundance ratios of V, Mn, and Co are larger than those of the even-$Z$ elements Ti, Cr, and Fe, respectively.

We see that [Sc/Fe], [Mn/Fe], and [Co/Fe] for $E_\nu = 9\times10^{53}$ and $3\times10^{54}$ ergs increase by 0.3–0.4 and 0.7–0.8 dex, respectively, compared with those for $E_\nu = 3\times10^{53}$ ergs. The total neutrino energies with $E_\nu = 9\times10^{53}$ and $3\times10^{54}$ ergs are 3 times and 10 times larger than that with $E_\nu = 3\times10^{53}$ ergs.

Simple consideration leads to the indication that the abundances of odd-$Z$ elements produced through the $\nu$-process are proportional to the neutrino flux, i.e., the total neutrino energy. Numerical simulations of the $\nu$-process show that this property is approximately correct. The reaction rates of the $\nu$-process are proportional to the total neutrino energy. At the same time, production rates of protons and neutrons produced through the $\nu$-process are also proportional to the total neutrino energy. The increase in the production rates brings about the increase in the production of odd-$Z$ elements through proton and neutron captures. However, the decomposition rates of the odd-$Z$ elements through proton and neutron captures also increase. Thus, the abundances produced through the $\nu$-process increase less than proportionally to the total neutrino energy.

We compare the obtained [Sc/Fe], [Mn/Fe], and [Co/Fe] with the corresponding observed results. The observed [Sc/Fe] averaged over 22 low-mass EMP stars is 0.06. This value is slightly larger than the solar ratio and is still much larger than the calculated abundance ratio even in the case of the largest neutrino irradiation. For Mn, the observed [Mn/Fe] is −0.43. This abundance ratio is larger than the ratio without the $\nu$-process and is reproduced by the result with the $\nu$-process with normal neutrino irradiation ($E_\nu = 3\times10^{53}$ ergs). On the other hand, the Mn/Fe ratio in the case of $E_\nu = 3\times10^{54}$ ergs is much larger than the largest value in the observed ratios. The observed [Co/Fe] is 0.31, which is larger than the solar ratio. It is larger than the value in the SN model even with the largest neutrino irradiation.

### 4.2. 25 $M_\odot$ *Supernova*

Figure 5 shows the abundance ratios of the 25 $M_\odot$ SN model. When we do not consider the $\nu$-process, the abundance ratios of Sc, Mn, and Co are much smaller than the corresponding solar ratios (see also Table 1). The $\nu$-process also enhances the production of these elements. When we consider the $\nu$-process, the Sc/Fe ratio in this model is larger than that in the 15 $M_\odot$ SN model. This is because the seed nucleus of $^{45}$V, i.e., $^{44}$Ti, is abundantly produced in complete Si burning for the 25 $M_\odot$ SN. However, the Sc/Fe ratio is smaller than the observed ratio even in the case of the largest neutrino irradiation. On the other hand, the Mn/Fe ratio in this model reproduces well the observed ratio in the case with a $\nu$-process with normal neutrino irradiation. The model with the largest neutrino irradiation ($E_\nu = 3\times10^{54}$ ergs) overproduces the Mn. The observed Co/Fe ratio is reproduced by the 25 $M_\odot$ SN model with the largest neutrino irradiation, $E_\nu = 3\times10^{54}$ ergs; large neutrino irradiation is similarly required for the 15 $M_\odot$ SN case.

### 4.3. 25 $M_\odot$ *Hypernova*

Figure 6 shows the distribution of the abundance ratios of the 25 $M_\odot$ HN model with $E_{51} = 20$. In this model we considered mixing and fallback as described in § 2.1. When we do not consider the $\nu$-process, the [Sc/Fe] and [Mn/Fe] are −1.1 and −1.9, respectively (see also Table 1). The Mn/Fe ratio is much smaller than the corresponding ratios in the other two models. Mn is mainly produced in the Si/S layer without the $\nu$-process (see

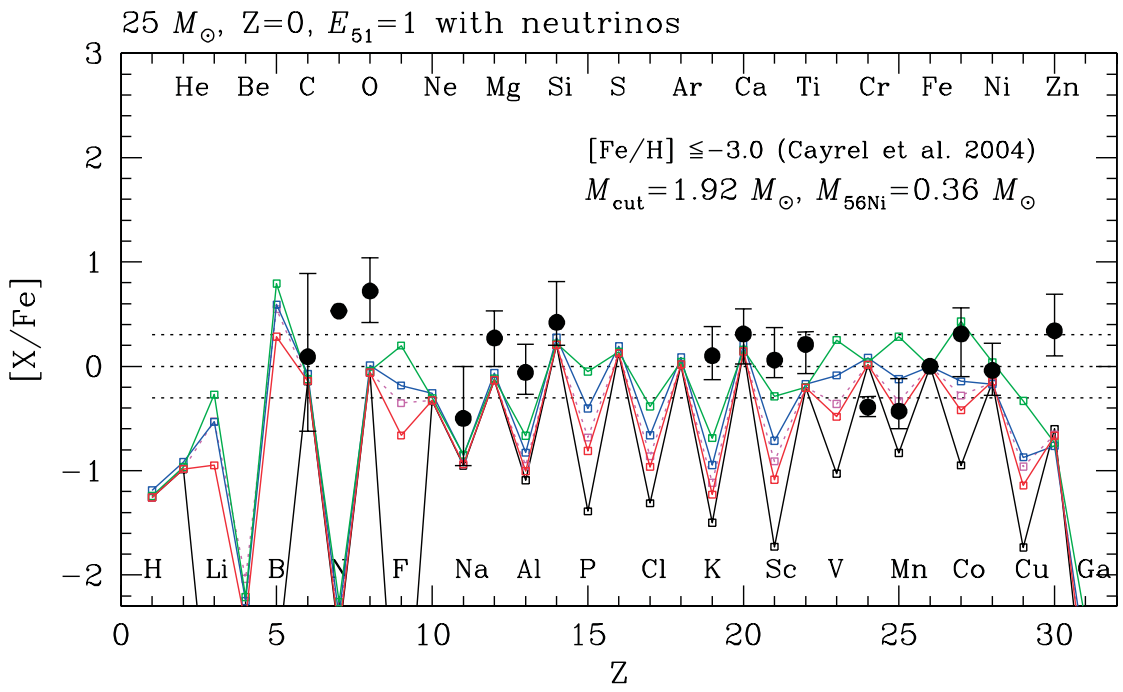


FIG. 5.—Same as Fig. 4, but for the SN of the 25 $M_\odot$ Population III star.

Fig. 3*a*), whereas the range of the Ni layer in the HN is larger than in the 25 $M_\odot$ SN. On the other hand, the Co/Fe ratio is larger than in the other SN models (see also Table 1). As shown in Figure 3*a*, the HN provides a large amount of Co through complete Si burning. The mass fraction of Co in the Ni layer is of order $10^{-4}$ for the 15 and 25 $M_\odot$ SN models, and $(2-3)\times10^{-3}$ for the 25 $M_\odot$ HN.

When we consider the $\nu$-process, the abundance ratios of Sc and Mn increase with the total neutrino energy. However, the Co abundance scarcely changes, even taking into account the $\nu$-process. The $\nu$-process raises the abundances of Sc and Mn in the Ni layer. Although it also enhances the Co abundance there, the contribution from the $\nu$-process is hindered by large Co production through complete Si burning.

We also compare our results with the observed ones. The obtained Sc/Fe ratio is smaller than the observed ratio. Even in the case of the largest neutrino irradiation, the abundance ratio is smaller by about 0.5 dex. The Mn/Fe ratio is marginally consistent with the observed ratio in the largest neutrino irradiation case. At the same time, the Co/Fe ratio is also marginally consistent with the observed ratio despite the $\nu$-process; the smallest Co/Fe ratio is reproduced. The HN model reproduces the observed

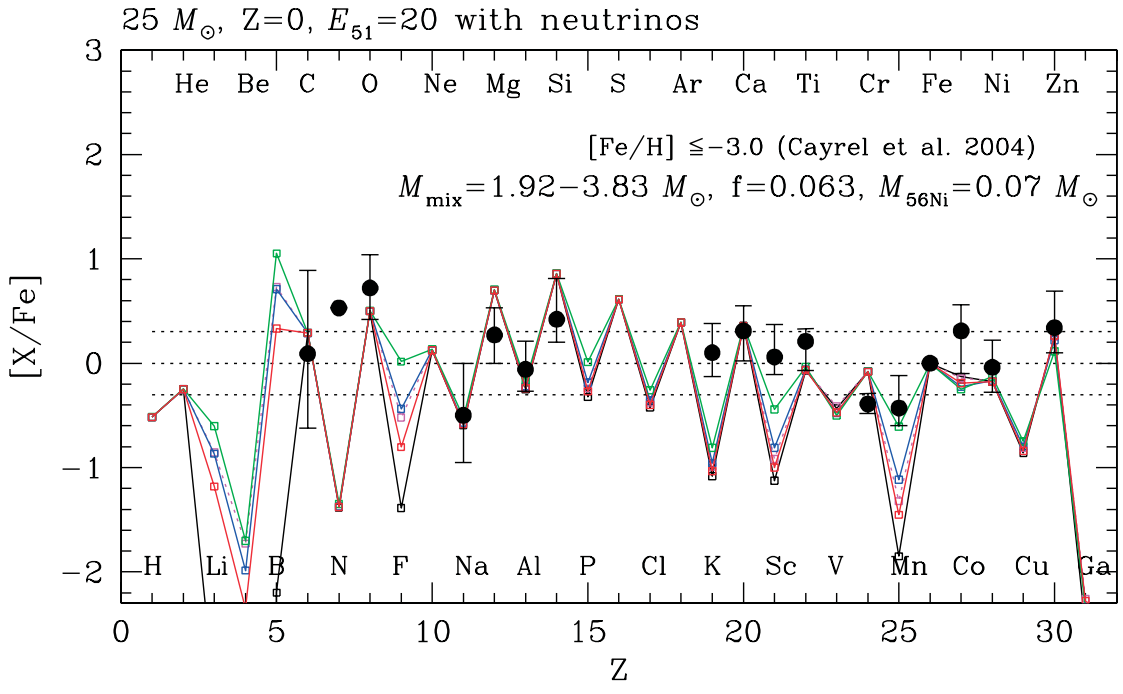


FIG. 6.—Same as Fig. 4, but for the HN ($E_{51}$ = 20) of the 25 $M_\odot$ Population III star.

Mn/Fe ratio when the $\nu$-process with large neutrino irradiation is taken into account. It reproduces the observed Co/Fe ratio even without the $\nu$-process.

When we do not consider the $\nu$-process, the abundance ratios of Sc/Fe, Mn/Fe, and Co/Fe in Population III SNe are smaller than the corresponding observed ratios. On the other hand, the observed Mn/Fe ratio is reproduced by the 15 and 25 $M_\odot$ SN models with the $\nu$-process. The observed Co/Fe ratio is marginally reproduced by the 25 $M_\odot$ HN model even without neutrino irradiation. Thus, we can say that the $\nu$-process in Population III SNe produce most of the Mn observed in low-mass EMP stars. The $\nu$-process also produces Sc, but the abundance is still too small to reproduce the observed Sc/Fe ratios. HNe may provide enough Co to reproduce the observed Co/Fe ratios.

### 4.4. $\nu$-Process with $T_\nu = 8$ MeV

We briefly mention the abundance ratios in the case of a $\nu$-process with $T_\nu = 8$ MeV and $E_\nu = 3 \times 10^{53}$ ergs, which has been adopted in WW95. The abundance patterns in the 15 and 25 $M_\odot$ SN and the 25 $M_\odot$ HN models are shown as dotted lines in Figures 4–6. The values of [Sc/Fe], [Mn/Fe], and [Co/Fe] are tabulated in Table 1. The yields of Sc, Mn, and Co in this neutrino parameter set are larger by about 0.1 dex than those in the case of $T_\nu = 6$ MeV. They are still smaller than those in the case of $T_\nu = 6$ MeV and $E_\nu = 9 \times 10^{53}$ ergs. Therefore, the dependence on the neutrino temperature is not strong for the Sc, Mn, and Co yields.

## 5. DISCUSSION

### 5.1. Abundance Pattern of VMP Stars

The abundance patterns of VMP stars are considered to reflect partly mixed interstellar materials in the early universe. Recently, the average abundance pattern of VMP stars with $-2.7 < [\mathrm{Fe/H}] < -2.0$ in Cayrel et al. (2004) has been reproduced by Population III SN and HN yields integrated over a Salpeter IMF function (Tominaga et al. 2007b). However, the evaluated [Sc/Fe] and [Mn/Fe] are still short of the observed ratio. We discuss the enhancement of these ratios by the $\nu$-process.

Tominaga et al. (2007b) evaluated the Sc/Fe ratio as $[\mathrm{Sc/Fe}] = -1.5$, whereas the observed value is $[\mathrm{Sc/Fe}] = 0.12^{+0.24}_{-0.14}$. In this study we showed that the $\nu$-process raises the Sc yield by 1.1 dex at the maximum. However, this enhancement is still small for reproducing the observed value. Production processes other than the $\nu$-process are needed to reproduce it (see § 5.2).

The [Mn/Fe] ratio observed in VMP stars is $-0.48^{+0.10}_{-0.24}$. The value of [Mn/Fe] in Tominaga et al. (2007b) is $-1.14$. When we take into account the $\nu$-process, this value increases by 0.24–0.4 dex with $E_\nu = 3 \times 10^{53}$ ergs and 0.49–0.73 dex with $E_\nu = 9 \times 10^{53}$ ergs. The increase from the $\nu$-process with $E_\nu = (3\text{–}9) \times 10^{53}$ ergs provides a better fit of Population III SN and HN yields of [Mn/Fe] in VMP stars.

The Population III SN and HN models in Tominaga et al. (2007b) indicate [Co/Fe] close to the lowest ratio in VMP stars; $[\mathrm{Co/Fe}] = 0.29^{+0.17}_{-0.27}$. Taking into account the $\nu$-process with $E_\nu = 3 \times 10^{53}$ ergs, [Co/Fe] increases by 0.37–0.53 dex in SNe, but not in HNe. This enhancement is enough to reproduce the average [Co/Fe] ratio in VMP stars. The $\nu$-process of Population III SNe and HNe is one of the preferred processes to produce the Mn and Co observed in VMP stars.

### 5.2. Other Production Sites of Sc, Mn, and Co

We have shown that Sc, Mn, and Co are produced through the $\nu$-process in Population III SNe and HNe. For elements other than Mn, the $\nu$-process in SNe and HNe does not produce large enough abundances to reproduce the abundances observed in low-mass EMP stars. So, we discuss other synthesis processes proposed in recent studies.

#### 5.2.1. Sc

##### 5.2.1.1. Aspherical Explosions

As shown in previous studies (e.g., Umeda & Nomoto 2002), spherically symmetrical SN and HN models do not provide enough Sc to reproduce the observed abundance in low-mass EMP stars. On the other hand, an aspherical explosion produces a larger amount of Sc (Maeda & Nomoto 2003). In the case of spherical explosions, low-density structure enables the supply of a larger amount of Sc (Umeda & Nomoto 2005). Thus, a higher temperature and lower density, which are realized by aspherical explosions, are a favorable environment for producing Sc. The amount of Sc produced in SNe and HNe is also sensitive to $Y_e$ in the complete Si-burning region. A large $Y_e$ value ($Y_e > 0.5$) brings about a large amount of Sc (Iwamoto et al. 2006).

##### 5.2.1.2. Nucleosynthesis in the Innermost Reions of SNe

The detailed thermal evolution of the innermost regions of SN ejecta, i.e., the region just above the "mass cut," has not been solved strictly. However, recent progress in hydrodynamical calculations has gradually revealed the thermal evolution in such deep regions. At the same time, detailed nucleosynthesis in such deep regions has also been investigated. Pruet et al. (2005, 2006) investigated the nucleosynthesis in convective bubbles in the innermost regions of SN ejecta and in the early stages of neutrino-driven winds. They used the results of the two-dimensional hydrodynamical calculations by Janka et al. (2003). Fröhlich et al. (2006b) examined the one-dimensional self-consistent simulations of core-collapse SNe with modified neutrino cross sections. They also investigated the nucleosynthesis in the innermost region just above the mass cut, solved self-consistently.

Both of the studies showed that the electron fraction $Y_e$ exceeds 0.5 in such regions, which enhances the production of Sc. In the latter study they took into account all charged-current weak interactions that change $Y_e$ in the ejecta. They obtained that $10^{-6}$ $M_\odot$ of Sc is produced in the innermost region when $Y_e > 0.5$. The Sc/Fe ratio evaluated in their study is slightly smaller than the average abundances observed in low-mass EMP stars (Cayrel et al. 2004). Thus, the Sc/Fe ratio is larger than our result. They also showed a significant amount of nuclei with mass $A > 64$ in this region, especially light $p$-nuclei such as $^{92,94}$Mo and $^{96,98}$Ru (the $\nu p$-process; Fröhlich et al. 2006a).

It is noted that the region with $Y_e > 0.5$ is convectively unstable, so the region will mix with the outer, smaller $Y_e$ region on a dynamical timescale. However, Fröhlich et al. (2006a) expected $Y_e$ to remain high in an average sense. Indeed, the former study took into account the convection in two-dimensional simulations and obtained $Y_e > 0.5$. We also note that neutral-current $\nu$-process reactions were not included in Fröhlich et al. (2006a, 2006b). They also pointed out that neutrino-induced spallation reactions can change the final abundances of some nuclei. We expect these reactions to enhance the abundance of Sc and the Sc/Fe ratio to become close to the observed ratio.

It is also noted that materials blown off in neutrino-driven winds at early times after a SN explosion can achieve a large $Y_e$ value. Accordingly, the $rp$-process can take place in the materials. This synthetic process is strongly preferred for the production of light $p$-nuclei (Wanajo 2006). However, the contribution of the $rp$-process in neutrino-driven winds to Sc production is small.

#### 5.2.2. Mn

The amount of Mn produced in SNe and HNe is strongly sensitive to the electron fraction $Y_e$ in the incomplete Si-burning region (Umeda & Nomoto 2002, 2005). Modifying the $Y_e$ value in their HN models to $Y_e \simeq 0.4995$–$0.4997$ produces enough Mn to reproduce that observed in low-mass EMP stars. However, HN models whose $Y_e$ in the incomplete Si-burning region was not modified indicated an amount of Mn less than the observed value. Aspherical explosions suppress Mn production (Maeda & Nomoto 2003). We have shown that the Mn production during SN explosions is mainly due to the $\nu$-process rather than to the incomplete Si burning. The $\nu$-process with normal neutrino irradiation ($E_\nu = 3 \times 10^{53}$ ergs) in SNe reproduces the Mn/Fe ratio averaged over low-mass EMP stars even without $Y_e$ modifications. In the case of $E_\nu = 9 \times 10^{53}$ ergs, the Mn amount marginally reproduces the upper limit of the observed Mn abundance. In the case of $E_\nu = 3 \times 10^{54}$ ergs, however, the SN models overproduce Mn. Thus, the $\nu$-process in Population III SNe is one of the main production processes of Mn observed in low-mass EMP stars. The observed abundance constrains the total neutrino energy $E_\nu$ in SNe. The observational constraint is $E_\nu \lesssim (3$–$9) \times 10^{53}$ ergs.

#### 5.2.3. Co

A large amount of Co can be produced through complete Si burning in an aspherical explosion (Maeda & Nomoto 2003). For spherical explosions, Umeda & Nomoto (2005) pointed out that the Co abundance is significantly enhanced for $Y_e > 0.5$ in the case of HNe. However, the Co/Fe ratio in Fröhlich et al. (2006b) is still smaller than the observed ratio in Cayrel et al. (2004). Their model corresponds to a normal SN explosion. Therefore, HNe ($E_{51} > 10$) with $Y_e \gtrsim 0.5$ produce an amount of Co that reproduces the observed Co/Fe ratio in low-mass EMP stars. Neutral-current $\nu$-process reactions may help additional production in the deep region just above the mass cut. However, in the case of HNe, a large amount of protons is also produced through $\alpha$-rich freeze-out. This effect may hinder the proton production by the $\nu$-process.

### 5.3. *Comparison with Other SN Nucleosynthesis Models*

Study of the nucleosynthesis in Population III SNe has been conducted by several groups. Here we briefly compare with the abundances of Sc, Mn, and Co for 15 and 25 $M_\odot$ Population III SN models in WW95WW95 (Z15A and Z25B models) and in Chieffi & Limongi (2004, hereafter CL04). The SN nucleosynthesis models in WW95 include the $\nu$-process. The temperature of $\nu_{\mu,\tau}$ in WW95 is assumed to be 8 MeV, which is larger than the one adopted in this study. SN nucleosynthesis with physics input updated from WW95 was shown in Rauscher et al. (2002), but Population III SN nucleosynthesis was not calculated. The nucleosynthesis models in CL04 do not include the $\nu$-process. The explosion models in CL04 set the ejected mass of $^{56}$Ni equal to 0.1 $M_\odot$.

WW95 indicate [Sc/Fe] $= -0.23$ for the 15 $M_\odot$ model; the Sc/Fe is much larger than our result. On the other hand, CL04 indicate Sc/Fe slightly larger than our results for SN models without the $\nu$-process ([Sc/Fe] $= -1.58$ for the 25 $M_\odot$ model). Although the Sc/Fe in WW95 is much larger than the other models, it is still smaller than the observed ratio. Therefore, other synthesis processes such as discussed above are necessary for Sc production.

The Mn/Fe shown in WW95 is smaller than the observed ratio ([Mn/Fe] $\leq -0.50$). The 15 $M_\odot$ model in CL04 also indicates an Mn/Fe smaller than the observed one ([Mn/Fe] $= -0.56$). The 25 $M_\odot$ model in CL04 indicates a larger Mn/Fe ratio, which is comparable to the observed one ([Mn/Fe] $= -0.33$). We showed that the $\nu$-process increases the Mn abundance, but a difference in stellar evolution models may affect the abundance.

The 15 $M_\odot$ models of WW95 and CL04 show [Co/Fe] values of $-0.22$ and $-0.11$, which are larger than the ratio of our SN models. Their 25 $M_\odot$ models indicate a Co/Fe ratio similar to our results without the $\nu$-process. The evaluated Co/Fe ratios are still short of the observed ratio, so HNe must have an important role for Co production in the early universe.

### 5.4. *The $\nu$-Process for Other Elements*

#### 5.4.1. Li *and* B

Among Li, Be, and B, $^7$Li and $^{11}$B are mainly produced through the $\nu$-process. When the $\nu$-process is not considered, the Li/Fe and B/Fe ratios are much smaller than the corresponding solar ratio. SN explosions with neutrinos of $E_\nu = 3 \times 10^{53}$ ergs bring about an Li yield ratio of [Li/Fe] $\gtrsim -1$. They also produce B, for which the yield ratio to Fe is larger than the solar ratio. Therefore, SN explosions may contribute to B production in the early universe. The $^7$Li is mainly produced as $^7$Be in the He-rich region. The $^{11}$B is produced as $^{11}$C and $^{11}$B in the C-enriched oxygen layer and the C-enriched He layer. The Li and B production in HNe is less effective than that in SNe. A higher maximum temperature in the He layer decomposes the $^7$Be and $^{11}$C produced through the $\nu$-process and the following $\alpha$-captures. In addition, a strong explosion makes the region of the C-rich oxygen layer small.

#### 5.4.2. F

The $\nu$-process is the main F production process in SNe (Woosley et al. 1990). The F/Fe ratio including the $\nu$-process is much larger than that without the $\nu$-process. The seed nucleus of F in the $\nu$-process is $^{20}$Ne. Most of the F is produced in the O- and Ne-enriched region. The stellar mass dependence of the F/Fe ratio is small in the SN models. On the other hand, the HN model shows a smaller F/Fe ratio. The HN explosion brings about stronger explosive Ne burning, so that the O- and Ne-enriched region becomes smaller.

#### 5.4.3. Na *and* Al

Figures 4–6 show that the $\nu$-process scarcely affects the yields of Na and Al. Furthermore, the yield ratios are much smaller than the observed ratios, even in the case of the largest neutrino irradiation. Although the $\nu$-process enhances the abundances of Na and Al in the incomplete Si-burning region, Na and Al are mainly produced in carbon and neon shells. The yields produced in the outer two shells strongly depend on the nucleosynthesis in the stellar evolution. Iwamoto et al. (2005) successfully reproduced the relatively large [Na/Fe] and [Al/Fe] ratios observed in two hyper-metal-poor stars. They considered the effect of overshooting during pre-SN evolution and extensive matter mixing and fallback during SN explosions with small explosion energies.

#### 5.4.4. V

Vanadium is mainly produced as $^{51}$Mn in the incomplete Si-burning region in SNe. In the case of the HN model, it is mainly produced in the complete Si-burning region. Additional production through the $\nu$-process from $^{52}$Fe in the incomplete Si-burning region contributes to the enhancement of V in SNe. Low-metallicity stars with $-3 \lesssim$ [Fe/H] $\lesssim -2$ indicate V abundance ratios of $-0.2 \lesssim$ [V/Fe] $\lesssim 0.6$ (e.g., Honda et al. 2004;

Kobayashi et al. 2006). The average abundance ratio is reproduced by the 15 and 25 $M_\odot$ SN models with the $\nu$-process of $E_\nu \sim 9 \times 10^{53}$ ergs. In order to reproduce the V/Fe ratios, strong neutrino irradiation in the SNe is favored. In the case of the HN model, V is also produced through the $\nu$-process. However, the produced abundance is much smaller than that produced in the complete Si-burning region.

## 6. SUMMARY

The chemical compositions of low-mass EMP stars are expected to be injected from one or a few SN or HN explosions of massive Population III stars. The abundance ratios of odd-$Z$ elements to Fe observed in these stars are close to the corresponding solar ratios. On the other hand, the abundances produced in complete and incomplete Si burning in SN explosion models are still too small.

In this study we investigated the $\nu$-process of the odd-$Z$ iron-peak elements Sc, Mn, and Co in the SN and HN explosions of 15 and 25 $M_\odot$ Population III stars. Then we compared the abundance ratios of these elements in the SN and HN models with those observed in EMP stars. The obtained results are summarized as follows.

1. Sc, Mn, and Co are produced through the $\nu$-process and the following capture reactions of protons and neutrons in the complete and incomplete Si-burning regions of Population III SNe. The produced amounts of these elements are roughly proportional to the total neutrino energy.

2. The observed Mn/Fe ratio averaged over low-mass EMP stars is reproduced by the 15 and 25 $M_\odot$ Population III SN models with the $\nu$-process. Therefore, the $\nu$-process in Population III SNe is one of the main synthesis processes of Mn observed in low-mass EMP stars. The observed Mn abundance constrains the total neutrino energy to $E_\nu \lesssim (3-9) \times 10^{53}$ ergs. This $E_\nu$ value is roughly consistent with the gravitational binding energy of a typical neutron star. In the case of the 25 $M_\odot$ Population III HN model, a large neutrino irradiation enables the reproduction of the observed Mn/Fe ratio.

3. The observed Co/Fe ratio is reproduced by the SN models. However, the required total neutrino energy is $E_\nu \sim 9-30$ ergs, which is larger than the typical value of the gravitational binding energy of a proto–neutron star. Complete Si burning in Population III HNe should be favorable to Co production rather than the $\nu$-process of SNe and HNe.

4. Although a larger amount of Sc is produced through the $\nu$-process, the Sc/Fe ratio is still smaller than the ratio observed in low-mass EMP stars.

5. Explosive nucleosynthesis during aspherical explosions and in a deep region just above the mass cut would be favorable to producing Sc and Co. The $\nu$-process and the capture reactions of protons and neutrons may also enhance the production of Sc, Mn, and Co in these environments.

We would like to thank the anonymous referee for valuable comments. Numerical computations were in part carried out on a general common-use computer system at the Astronomy Data Center (ADC) of the National Astronomical Observatory of Japan. This work has been supported in part by the Ministry of Education, Culture, Sports, Science, and Technology, Grants-in-Aid for Young Scientists (B) (17740130), and Scientific Research (S) (18104003), (C) (16540229 and 18540231). T. Y. was supported by the 21st Century COE Program "Exploring New Science by Bridging Particle-Matter Hierarchy" in the Graduate School of Science, Tohoku University.

## REFERENCES

Argast, D., Samland, M., Gerhard, O. E., & Thielemann, F.-K. 2000, A&A, 356, 873
Cayrel, R., et al. 2004, A&A, 416, 1117
Chieffi, A., & Limongi, M. 2004, ApJ, 608, 405 (CL04)
Colella, P., & Woodward, P. R. 1984, J. Comput. Phys., 54, 174
Domogatsky, G. V., Eramzhyan, R. A., & Nadyozhin, D. K. 1978, in Neutrino Physics and Neutrino Astrophysics, ed. M. A. Markov et al. (Moscow: Nauka), 115
Fröhlich, C., Martínez-Pinedo, G., Liebendörfer, M., Thielemann, F.-K., Bravo, E., Hix, W. R., Langanke, K., & Zinner, N. T. 2006a, Phys. Rev. Lett., 96, 142502
Fröhlich, C., et al. 2006b, ApJ, 637, 415
Goriely, S., Arnould, M., Borzov, I., & Rayet, M. 2001, A&A, 375, L35
Heger, A., Kolbe, E., Haxton, W. C., Langanke, K., Martínez-Pinedo, G., & Woosley, S. E. 2005, Phys. Lett. B, 606, 258
Hix, W. R., & Thielemann, F.-K. 1996, ApJ, 460, 869
Honda, S., Aoki, W., Kajino, T., Ando, H., Beers, T. C., Izumiura, H., Sadakane, K., & Takada-Hidai, M. 2004, ApJ, 607, 474
Iwamoto, N., Umeda, H., Nomoto, K., Tominaga, N., Thielemann, F.-K., & Hix, W. R. 2006, in International Symposium on the Origin of Matter and Evolution of Galaxies 2005, ed. S. Kubono et al. (San Francisco: AIP), 409
Iwamoto, N., Umeda, H., Tominaga, N., Nomoto, K., & Maeda, K. 2005, Science, 309, 451
Janka, H.-T., Buras, R., & Rampp, M. 2003, Nucl. Phys. A, 718, 269
Kobayashi, C., Umeda, H., Nomoto, K., Tominaga, N., & Ohkubo, T. 2006, ApJ, 653, 1145
Kotake, K., Sawai, H., Yamada, S., & Sato, K. 2004, ApJ, 608, 391
Lattimer, J. M., & Prakash, M. 2001, ApJ, 550, 426
Maeda, K., & Nomoto, K. 2003, ApJ, 598, 1163
McLaughlin, G. C., & Surman, R. 2007, Phys. Rev. D, 75, 023005
Nomoto, K., Tominaga, N., Umeda, H., Kobayashi, C., & Maeda, K. 2006, Nucl. Phys. A, 777, 424
Norris, J. E., Ryan, S. G., & Beers, T. C. 2001, ApJ, 561, 1034
Pruet, J., Hoffman, R. D., Woosley, S. E., Janka, H.-T., & Buras, R. 2006, ApJ, 644, 1028
Pruet, J., Woosley, S. E., Buras, R., Janka, H.-T., & Hoffman, R. D. 2005, ApJ, 623, 325
Rauscher, T., Heger, A., Hoffman, R. D., & Woosley, S. E. 2002, ApJ, 576, 323
Scheck, L., Plewa, T., Janka, H.-T., Kifonidis, K., & Müller, E. 2004, Phys. Rev. Lett., 92, 011103
Shigeyama, T., & Tsujimoto, T. 1998, ApJ, 507, L135
Tominaga, N., Maeda, K., Umeda, H., Nomoto, K., Tanaka, M., Iwamoto, N., Suzuki, T., & Mazzali, P. 2007a, ApJ, 657, L77
Tominaga, N., Umeda, H., & Nomoto, K. 2007b, ApJ, 660, 516
Tominaga, N., et al. 2005, ApJ, 633, L97
Umeda, H., & Nomoto, K. 2002, ApJ, 565, 385
———. 2005, ApJ, 619, 427
Wanajo, S. 2006, ApJ, 647, 1323
Woosley, S. E., Hartmann, D. H., Hoffman, R. D., & Haxton, W. C. 1990, ApJ, 356, 272
Woosley, S. E., & Weaver, T. A. 1995, ApJS, 101, 181 (WW95)
Yoshida, T., Kajino, T., & Hartmann, D. H. 2005a, Phys. Rev. Lett., 94, 231101
Yoshida, T., Kajino, T., Yokomakura, H., Kimura, K., Takamura, A., & Hartmann, D. H. 2006a, ApJ, 649, 319
———. 2006b, Phys. Rev. Lett., 96, 091101
Yoshida, T., Terasawa, M., Kajino, T., & Sumiyoshi, K. 2004, ApJ, 600, 204
Yoshida, T., Umeda, H., & Nomoto, K. 2005b, ApJ, 631, 1039